JOURNAL OF AIRCRAFT
Vol. 46, No. 4, July–August 2009

Inverted Jet Spoilers for Aerodynamic Control

Antonio Filippone*
University of Manchester, Manchester, England M60 1QD, United Kingdom

DOI: 10.2514/1.40321

This paper reviews concepts for flow control based on jet spoilers and presents a new device based on the jet principle for application to fixed-wing aircraft. The new concept relies on the naturally blown inverse spoiler. The jet is blown parallel to the surface and points against the freestream. The theoretical basis of the device is presented. Calculations are performed with a Navier–Stokes program to investigate the key design parameters. These parameters include the spoiler deflection (equal or differential), the position of the hinge points, the shape of the bypass channel, the effects of backward- and forward-facing steps in a partial deflection, and the nature and magnitude of the control forces. A comparison is done with conventional inlay spoilers. Finally, a multidimensional optimization has been carried out to study the combined effects of hinge position, deflection, and spoiler length. Optimal configurations with respect to jet momentum and drag coefficient have been analyzed.

Nomenclature

C_d	=	drag coefficient
C_l	=	lift coefficient
C_m	=	pitching moment coefficient
C_p	=	pressure coefficient
C_μ	=	jet momentum coefficient
c	=	airfoil chord
D	=	aerodynamic drag
F	=	force
l	=	spoiler's length
M_h	=	hinge moment
$\dot{m}$	=	mass flow rate
n	=	number of cells in a given direction
P	=	pressure
q_∞	=	freestream dynamic pressure
Re	=	Reynolds number
t	=	time
$\mathbf{U}$	=	velocity vector
U_1	=	inviscid velocity at inlet of bypass
U_∞	=	freestream velocity
x_{LE}	=	position of spoiler's leading edge
x_h	=	hinge position
α	=	angle of attack
δ	=	spoiler deflection
η, ξ	=	local reference system
ρ	=	air density

Subscript

j	=	jet quantity

Superscripts

$+$	=	upper spoiler
$-$	=	lower spoiler

Received 8 August 2008; accepted for publication 10 October 2008.

*Senior Lecturer, School of Mechanical, Aerospace and Civil Engineering, George Begg Building, P.O. Box 88; a.filippone@manchester.ac.uk. Senior Member AIAA.

I. Introduction

AERODYNAMIC flow control on aircraft wings is achieved in a variety of ways. The trailing-edge slotted flaps are general control devices for increasing the lift in low-speed maneuvers. Roll control can be achieved with ailerons; these are panels that can be deflected up and down. The term *spoiler* is generally given to any upper-surface-deployable panel. The conventional spoilers open up like hatch doors to about 90 deg. If they are deployed in the ground run, the spoilers are used as lift dumpers and speed brakes. Aerodynamic braking can also be achieved by a split aileron that operates as a clamshell. Although this device is quite effective, it requires large moments to be operated. As a consequence, a relatively large auxiliary power is required. If the spoilers are used in flight, they will cause the aircraft to pitch up. If used differentially, they cause a yawing moment. The use of spoilers for lateral and longitudinal control in flight has been of interest to aircraft designers for a number of years. The spoilers are in fact used over a wide range of speeds and are known to contribute a large portion of lateral control power. This field is now ripe with ideas requiring detailed analysis and exploitation.

Blake [1] described a spoiler design for yaw control of a tailless aircraft. This concept is illustrated in Fig. 1. The inverse spoiler is called the *deflector*. Yaw control is achieved by differential deflection actuated by a kinematic linkage with pivots and arms. The entire system is designed to be mounted within the wing and to be integrated with the flight control system. It is claimed that the device features a greatly reduced radar signature, but its main function is to provide yaw control. In the configuration shown in Fig. 1, the forward deflection of the top spoiler diverts the flow away from the wing, and the lower spoiler directs the flow into the wing. Therefore, a given yaw moment can be achieved with relatively small control forces.

Clark [2] described a similar forward-opening spoiler, designed for applications to all-wing aircraft. As in the previous case, the main motivation of this application is a reduced radar signature for tailless aircraft, although yaw control without down force is its main requirement. For example, a conventional inlay spoiler requires an inverted lower spoiler to eliminate the downforce created by the top spoiler. The net effect is claimed to feature an increased drag without a loss in lift.

Because these basic ideas are protected by intellectual property, it is not possible to make a technical assessment of their claims. In particular, it is not possible to assess their viability, their function, and their side effects on both the systems themselves and the aircraft as a whole. One item of particular interest in the context of the present analysis would be the amount of spoiler deflection required for achieving a defined control value.

Tavella et al. [3,4] described two airfoil blowing systems for roll and yaw control. These systems are based on the concept that control

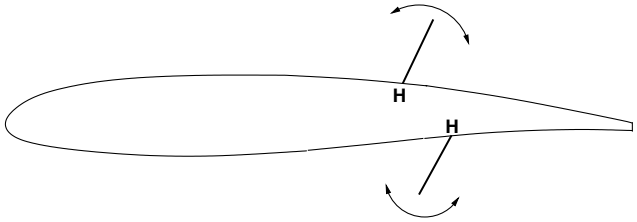

Fig. 1 Yaw control device according to Blake [1]; H denotes the hinge position.

would be best done without deflecting solid surfaces; hence, they are based on jet blowing techniques. Jet spoiler blowing can be used to create differential lift and drag and thus yawing moments. Among other things, the maximum efficiency of the device is achieved when the jet blowing is placed at the position of maximum thickness of the airfoil (Fig. 2).

A similar concept has been devised for a Darrieus wind turbine [5]. In this concept, the airfoil is hollow and has a central chamber that feeds air to the opening on the surface. The jet is used for controlling flow separation (for example, by forcing airfoil stall), thereby reducing the net output power. The system requires a feedback control unit that uses external power.

This idea has been developed further by McClure [6], who devised a method for creating a jet by using internal channels, as shown in Fig. 3. The inlet is at the lower part of the leading edge. Relatively-high-pressure air is conveyed inside the channel and then split in two jets (upper and lower) in the rear part of the airfoil. This concept does not consider the limitations that may occur in the manufacturing of the device: namely, the fact that the internal channel would have to run through the wing spars. Furthermore, the amount of air that can be extracted at the inlet is limited. Only weak and uncontrollable jets are produced at the outlet. It is unlikely that this device can be used for any useful purpose, also as a result of the pressure losses in the long internal channel.

The conventional inlay spoilers have been investigated experimentally and computationally over a number of years. There is now a body of work on issues such as unsteady aerodynamics during deflection [7] and nonlinear control [8]. Lee and Bodapati [9] published aerodynamic data and an analysis of the flow characteristics; Consigny et al. [10] analyzed the aerodynamic performance of rapidly-deploying spoilers. These latter studies did not focus on lateral control. These studies show that at moderate-to-high spoiler deflection, the lift becomes negative. This is useful in the ground run to increase the rolling resistance.

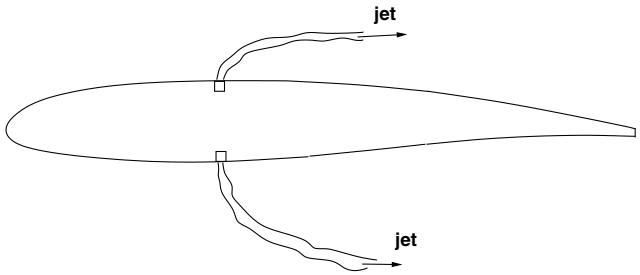

Fig. 2 Yaw control device according to Tavella et al. [4]

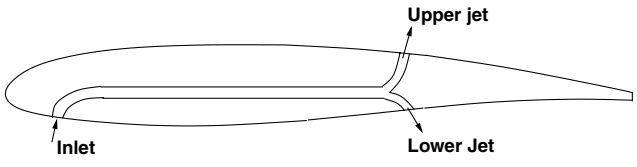

Fig. 3 Yaw control device according to McClure [6].

II. New Spoiler Concept

In this paper we propose to investigate the effects on the aerodynamic lift, pitching moment, roll moment, and yaw moment on an aircraft wing at low-to-moderate air speeds. This control can be obtained by means of cavities that are exposed to the flow by operating an internal mechanism (electric or otherwise). The mechanism opens and closes panels aligned with the wing. There are three basic models, but only one has been investigated and presented in this paper (Mark III). This device is shown in Fig. 4.

The bypass is not necessary for the operation of the spoiler, but its presence creates a peculiar aerodynamic response and perhaps alleviates problems such as vibrations caused by flow into the wing. Conveniently, Clark's concept (Fig. 1) is canted to let air flow out of the spoiler, because stagnating flow can be unsteady and leads to forced vibrations. In the configuration proposed, there is no stagnating flow. The lift is generally positive, albeit rather small, and therefore a straightforward comparison with the inlay spoilers cannot be done. An increase in drag is required in certain maneuvers, such as braking upon landing, and to increase the terminal-area descent rate [11].

The main geometrical parameters are the hinge position of the upper and lower spoilers, length of the upper/lower spoilers, angle of deflection of the upper/lower spoilers, width of the cavities, and geometry of the U-bend between the spoiler cavities. When the spoiler is mounted on a wing, there are three additional parameters to consider: spanwise position, spanwise dimension, and number of spoilers.

The shape of the bypass channel affects the internal flow and the flow at the exit of the upper spoiler: in particular, the viscous losses and the blockage due to flow separation at the inlet, outlet, or U-bend. The assembly (including the control mechanism) can be pushed back toward the trailing edge to leave room for the wing spar. Because the device must ultimately be operated through an internal mechanism (as described in Fig. 4), it is important to evaluate the forces required to open/close, the relationship between a deflection and the aerodynamic response, and the added weight. Two basic control mechanisms are envisioned: one is based on electric power and the other is based on a cam shaft, which requires the application of a torque to create the sliding of a cam into the spoiler assembly. Both mechanisms may require further improvement if differential deflection of the spoilers is required.

We consider two options: in the first case, the spoiler can assume only two positions: open or closed (simple bypass version); in the second case, the deflection is continuous from closed to fully open (slotted bypass version). The latter case is more general and allows a larger degree of aerodynamic control; it is discussed in Secs. IV.C and IV.F.

Spoilers can be used in multiple sections. For example, outboard spoilers can be used for lateral maneuvers and inboard spoilers can be used for aerodynamic breaking. When a high drag is required, the spoilers effectively operate as clamshells. The internal flow is caused by the difference in pressure between the lower and upper sides. An increase in bypass flow is further facilitated by the loss of pressure on the upper side, which is due to local accelerations of the flow. If the bypass flow rate is $\dot{m}$, the increase in drag due to the bypass is calculated by the change streamwise in momentum:

$$\Delta D = \mathbf{F} \cdot \mathbf{i} = \dot{m}(\mathbf{U}^+ - \mathbf{U}^-) \cdot \mathbf{i} \tag{1}$$

where $\mathbf{F}$ is the total aerodynamic force caused by the bypass, $\mathbf{U}^-$ is the average inlet velocity, $\mathbf{U}^+$ is the average outlet velocity, and $\mathbf{i}$ is the unit vector in the streamwise direction. Thus, it appears that to

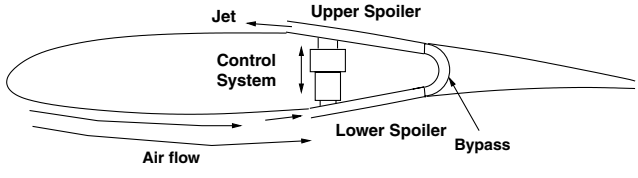

Fig. 4 Upper and lower spoilers with internal bypass (Mark III).

increase the drag one must increase the mass flow rate and the difference between inlet and outlet velocity in the bypass. For a given deflection, the mass flow rate increases with the jet speed; for a given jet speed (or fixed pressure difference at the ends of the channel), the mass flow rate should increase with the amount of deflection. This is not always true, as discussed further in the results. However, in the configuration proposed there is a practical limit to the deflection of the spoilers, because the slots must be allocated within the wing section.

Along with the bypass flow, a second effect must also be considered. In fact, the bypass flow creates a jet on the upper side of the wing. The jet may cause flow separation both upstream and downstream of the spoiler's leading edge. Flow separation causes an increase in drag and a decrease in lift. Unlike other concepts reviewed earlier, this jet is parallel to the wall. Furthermore, because the jet relies only on natural differences in pressure at the two ends of the channel, the jet will be weaker than those obtained with external power. The jet momentum coefficient is defined as

$$C_\mu = \frac{\rho_j U_j^2 \delta_j}{q_\infty c} \tag{2}$$

where the subscript j denotes the jet (at the exit of the bypass), δ_j is the thickness of the jet (or the spoiler's deflection), q_∞ is the freestream dynamic pressure and c is the chord. A first-order estimation of the C_μ can be found from inviscid theory across the bypass. Under this simplified case, the jet velocity is

$$U_j^2 = \frac{\Delta p}{\rho} - U_1^2 \tag{3}$$

where U_1 is the velocity at the inlet of the bypass and Δp is the difference in pressure between the inlet and the outlet. In Eq. (3), Δp is the pressure difference between the inlet and the outlet of the bypass. In terms of the pressure coefficient for a unit-chord wing, we have

$$C_\mu \simeq 2\left[\Delta C_p - \left(\frac{U_1}{U_\infty}\right)^2\right]\frac{\delta_j}{c} \tag{4}$$

Equation (4) represents an upper limit of the C_μ that can be produced. The term ΔC_p increases with α, whereas U_1/U_∞ decreases. Viscous effects, flow separation inside the bypass, and the merging of the jet with the incoming stream all contribute to some loss of momentum. However, this equation is useful because it allows a preliminary design of the device with a constraint of maximum momentum coefficient for a given airfoil section and inflow conditions. For the supercritical wing section NASA SC-20712 (12% thick) at low subsonic speeds, with an inlet and outlet both placed at $x/c = 0.70$, the theoretical C_μ is estimated by the following equation:

$$C_\mu \simeq (1.618 - 0.295\alpha)\delta_j \tag{5}$$

where α is the angle of attack in degrees. The coefficients of the equation change if the reference point is moved. Equation (5) is calculated from two-dimensional airfoil theory, first by evaluating the C_p and the U_1/U_∞ at specified locations, then by calculating Eq. (4). Thus, for a 1% spoiler deflection, one could expect $C_\mu \simeq 1.6 \times 10^{-2}$ in the absence of viscous losses in the bypass. However, these losses can be substantial, and the effective C_μ can be reduced by as much as 1 order of magnitude, as demonstrated by the computational analysis.

III. Computational Model

The analysis of the spoiler's aerodynamic performance was done with an unsteady Reynolds-averaged Navier–Stokes (URANS) code with appropriate turbulence closures. The wing considered was the NACA supercritical section SC-20712. This section was modified at the aft portion ($x/c > 0.5$) to close the trailing-edge gap. A sharp trailing edge simplifies the grid generation and does not affect the overall performance of the wing section with spoilers deployed. A panel-method solution of the flow past the wing section was used to generate the wake line; on turns, the wake was used as a baseline for the outer-grid generation.

A grid generator was programmed for this scope; the program generates an outer C-type mesh by solving hyperbolic equations and an inner O-type mesh by transfinite interpolation. The contour of the U-bend between the upper and lower spoilers was generated by using cubic Bezier splines because, in general, it is not possible to connect the spoilers with circular arcs. The width of the channel at the center of the U-bend was a free parameter (considered separately). The final mesh consisted of 14 structured blocks, each having $n \times n$ cells. An automatic block-splitting technique was added to the program. Grid resolution studies have been performed by changing the number of cells n. Two streamwise blocks were used in the wake (e.g., $2n$ spanwise cells); two blocks were in the bypass channel; and five blocks were on the wing section, which gave a total of $5n$ cells around the contours. Values used for n ranged from 36 to 68.

An example of this grid is shown in Fig. 5a, which is a cut through the middle of the slots. The wing appears to be split in two parts. However, this is not the case in a practical three-dimensional wing, due to the limited spanwise extent of the spoilers. Another detail worth mentioning is that the spoilers have a finite thickness. This has been programmed in the construction of the geometrical model. This detail is presented in Fig. 5b, which also shows the position of the hinges and the geometry of the bypass for a particular spoiler configuration.

The flow solver used is a two-dimensional version of a solver used in the past for aerodynamic flows over a variety of applications [12–16]. The flow solver is optimized for message-passing interface and is capable of running efficiently on multiprocessor computers.

The convective terms are discretized using a second-order total-variation-diminishing upwind scheme. Central differences are used

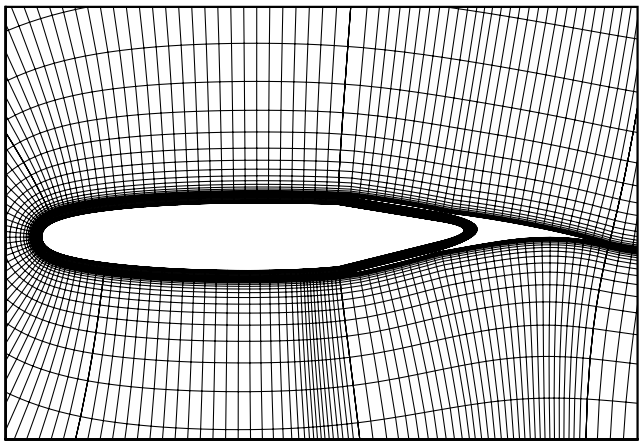

a) Airfoil grid

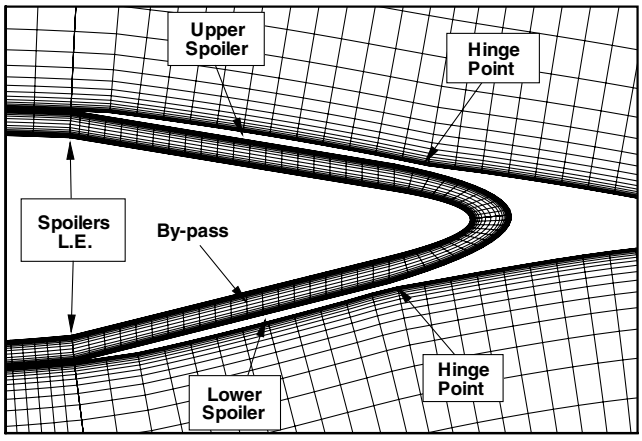

b) Grid around bypass

Fig. 5 Two-dimensional grid around Mark III spoilers; $x_h = 0.70$.

for the viscous terms. Only the normal terms are treated fully implicit; the other terms are treated explicitly. The pressure and velocity coupling is obtained through the SIMPLE algorithm. The momentum equations are solved by using a predictor–corrector method to advance the solution in time. The two-step procedure corresponds to a single iteration. The two momentum equations are solved by using a red/black Gauss–Seidel point solver. The solution of the elliptic Poisson system arising from the pressure-correction equation is accelerated using a multigrid method. The use of square blocks $n \times n$ further accelerates the computational performance of the Poisson solver; in fact, unsteady solutions could be obtained on a single-processor desktop computer in a matter of 40 to 60 min.

This excellent solver performance allows a relatively quick computation of the parametric effects. The software was run on a workstation by invoking a batch script. The script reads an input file, calls the grid generator, the solver's preprocessor (to build the communication tables), the flow solver itself, and the postprocessor and dumps the resulting data in a separate folder; then it starts the procedure with updated parameters.

Although this procedure generally works, it is possible that the grid generated for some cases is suboptimal; the flow solver diverges and the entire process comes to a halt. Therefore, the grid has to be improved manually. This case is discussed further in the optimization analysis (Sec. IV.F).

The turbulence model used for the analysis presented was a low-Reynolds-number k-ω shear-stress tensor model. Numerical studies performed by Choi et al. [17] indicate that two-equation turbulence models are adequate for engineering calculations of separated flows past inlay spoilers that are fixed or rapidly moving. This aspect of the turbulence effects was not investigated any further, except in those cases for which a change in underrelaxation avoided convergence overflow on the turbulent quantities.

To understand the aerodynamic performance of the device, a number of numerical tests have been run to check the consistency of the results. One test consisted of a grid refinement study for a given spoiler configuration. A two- or three-multigrid approach is required for the spoiler configuration. The cases showed in this paper are converged to 10^{-5} or 10^{-6} (or less) for momentum and continuity equations and turbulence equations. An example is shown in Fig. 6. All of the cases shown in the following analysis have a similar trend; in particular, the wavy features in the residual are always present. These waves could not be associated with any particular flow feature.

Figure 7 shows the convergence on the C_μ for three different grid sizes (as indicated). The time step for these cases was $\Delta t = 0.8 \times 10^{-3}$ s at $Re = 3 \times 10^6$ and $\alpha = 0$. The geometrical parameters were $\delta^+/c = \delta^-/c = 0.012$ and $x_h^+/c = x_h^-/c = 0.70$. A flow time $Ut/c \simeq 2$ is required for the momentum coefficient to stabilize to a constant level. The change in C_μ at $n = 68$ and above was considered to be negligible; thus, the analysis shown in this study was done with a mesh size $n = 68$, which corresponds to 64,736 cells in the integration domain, and this includes 136 cells in the wake and 68 cells across the bypass.

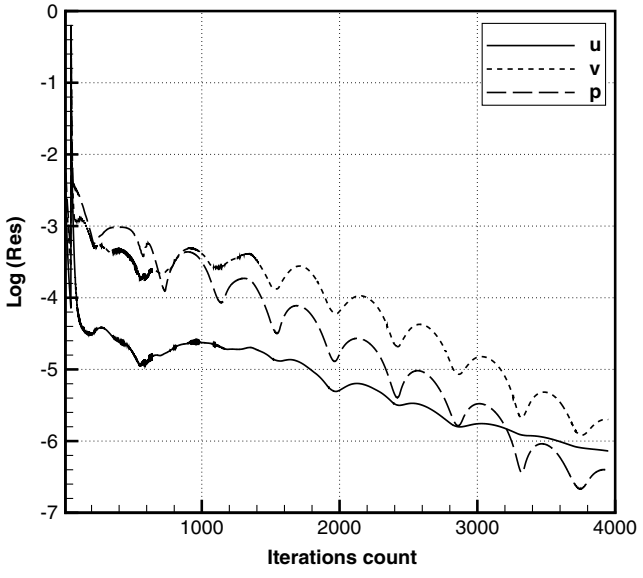

Fig. 6 Typical residual history.

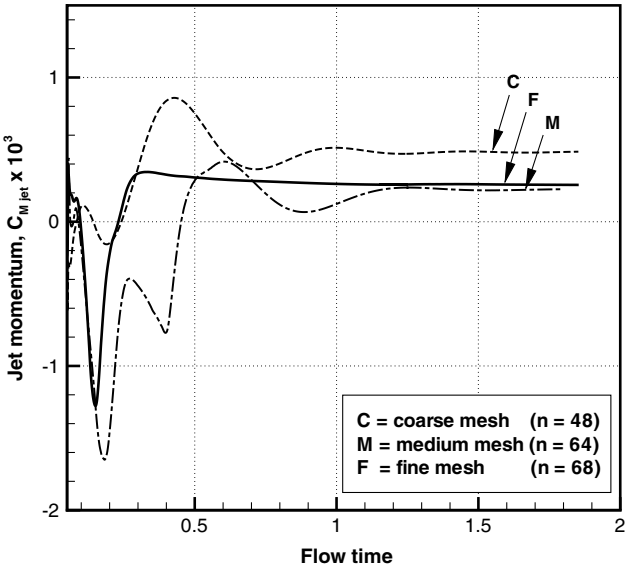

Fig. 7 Effect of grid refinement on jet momentum coefficient.

A further numerical test was done on a supercritical wing equipped with a conventional inlay spoiler to study the capability of the flow solver in the presence of massive flow separation. Figure 8 shows a comparison with some wind-tunnel data extracted from Consigny et al. [10] and further described by Choi et al. [17]. The wing section used was a 16%-thick supercritical wing (ONERA RA16SC) at $\alpha = 0$ deg, $M = 0.30$, and $Re = 1.9 \times 10^6$, with an inlay spoiler hinged at $x/c = 0.52$ and deflected by $\delta = 20$ deg. The computational model consisted of 20 blocks with $n = 64$, giving a total grid size of 81,920 cells. The solution was advanced to $Ut/c \simeq 5$ with a time step $\Delta t = 0.5 \times 10^{-3}$.

The overall agreement is satisfactory, although the present solution failed to produce a more gradual pressure recovery on the lee side of the spoiler. This discrepancy was attributed to the different geometrical details. In fact, the experimental setup consisted of a thick spoiler that left a cavity and a gap when it was deflected. This

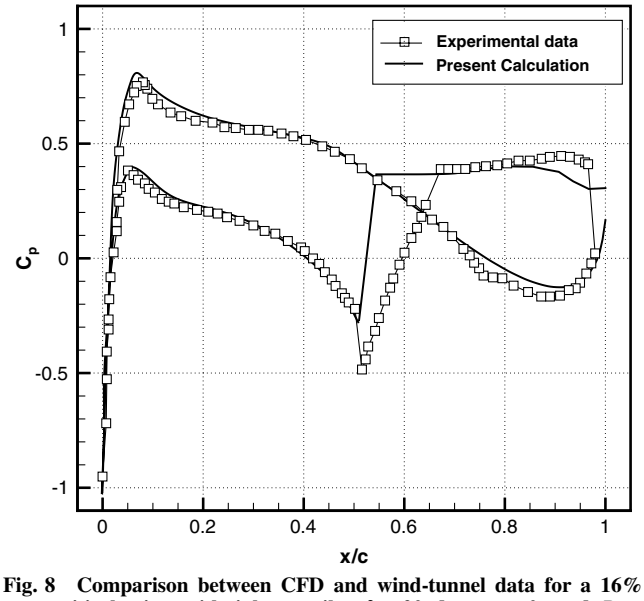

Fig. 8 Comparison between CFD and wind-tunnel data for a 16% supercritical wing with inlay spoiler $\delta = 20$ deg, $\alpha = 0$, and $Re = 1.9 \times 10^6$.

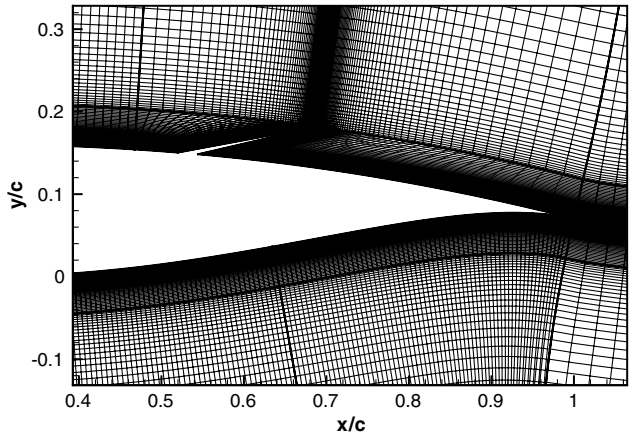

Fig. 9 Grid around inlay spoiler; $\delta = 20$ deg.

cavity was not modeled, as shown in Fig. 9. The spoiler in the computational fluid dynamics (CFD) model was a wedge plate with its root on the wing surface.

IV. Results and Analysis

When preparing for the aerodynamic analysis and optimization of the jet spoilers, one has to determine the relevant performance parameter. This, in fact, depends on the type of control that is to be achieved and the type of application. A typical analysis involves the net drag, pitching moment, or lift deficiency with respect to the basic wing configuration. These forces and moments can be combined on the three-dimensional wing to provide the desired control. It is also of some interest to evaluate the net jet effect, or the jet momentum coefficient, as a function of the relevant parameters. The analysis starts from the evaluation of the jet momentum coefficient and the effect of the main geometrical parameters. All of the data discussed refer to a Reynolds number $Re = 3 \times 10^6$.

A. Effect of Spoiler Deflection

For a given spoiler configuration, aerodynamic control can be achieved by opening and closing the spoiler. This can be done in at least two ways: 1) by simultaneous opening by the same amount δ (at the leading edge) and 2) by differential deflection by the amount δ^+ (top spoiler) and δ^- (bottom spoiler). The amount of deflection is limited by the dimension of the wing section and the spoiler. The analysis presented was performed with deflections δ/c, variable between 0.6 and 1.4%.

The first case, relative to equal deflection around a hinge at $x_h/c = 0.70$, is shown in Fig. 10. The calculations are shown for a limited range of angles of attack. The computed data are fitted with third-order polynomial curves. The maximum jet momentum is achieved with a deflection of about 1% chord. The maximum value of C_μ is 1 order of magnitude lower than the value predicted by Eq. (5). As the spoilers are open wide, the flow inside the bypass channel is affected by crosswise velocity gradients that create separation both at the inlet and the outlet.

For a given configuration, this flow separation must be avoided to get a higher momentum out of the upper spoiler. On the other hand, when the spoilers have a narrow deflection, the net mass flow is limited by the cross-sectional area. The effect of angle of attack is relatively weak for small positive angles of attack of the wing. This behavior is consistent with the fact that as the difference in pressure between the lower and upper spoilers increases (by increasing α), so does the mass flow rate through the bypass. The effect of the deflection follows the trend of $\alpha = 0$. The computed C_l and C_d are shown in Fig. 11.

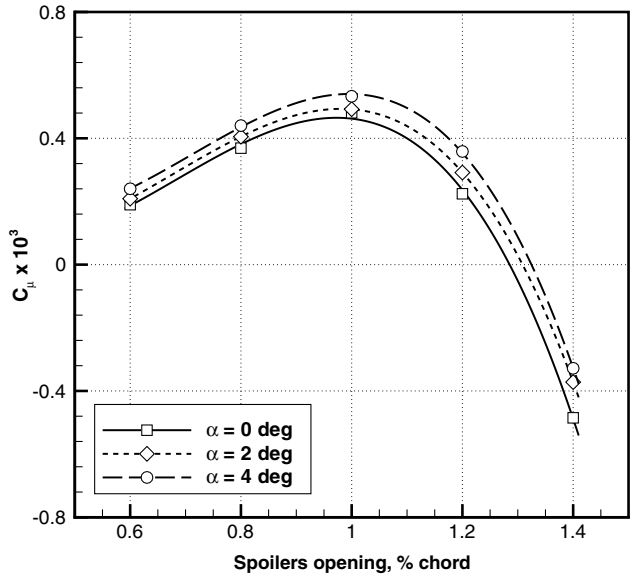

Fig. 10 Effect of simultaneous deflection on net jet momentum.

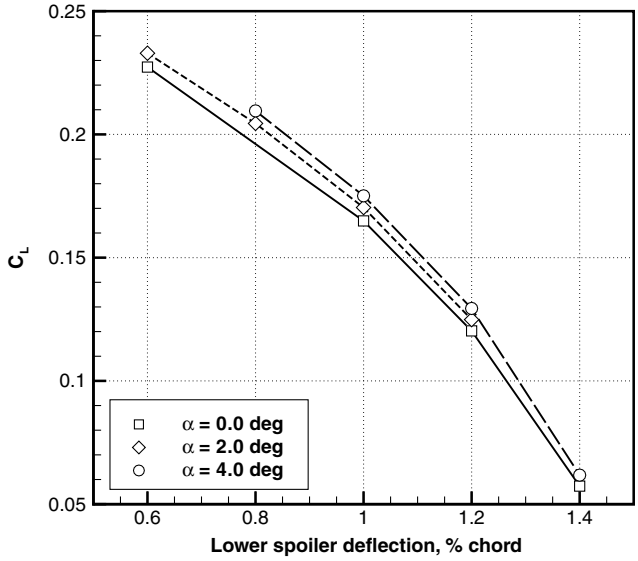

a) Lift coefficient

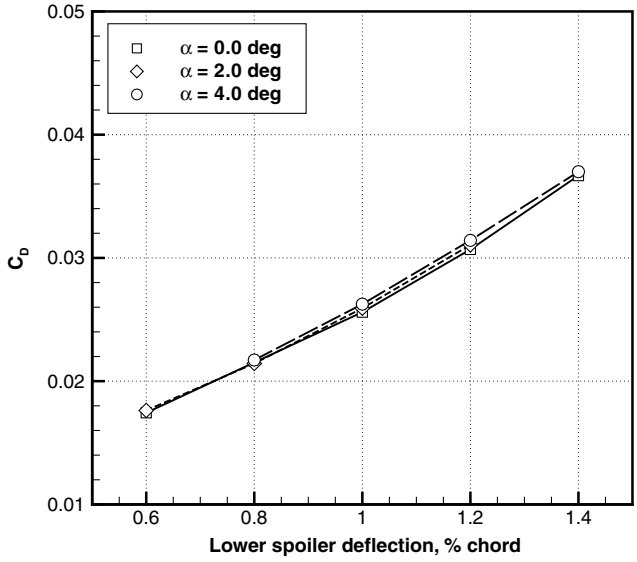

b) Drag coefficient

Fig. 11 Effect of simultaneous deflection on net aerodynamic coefficients.

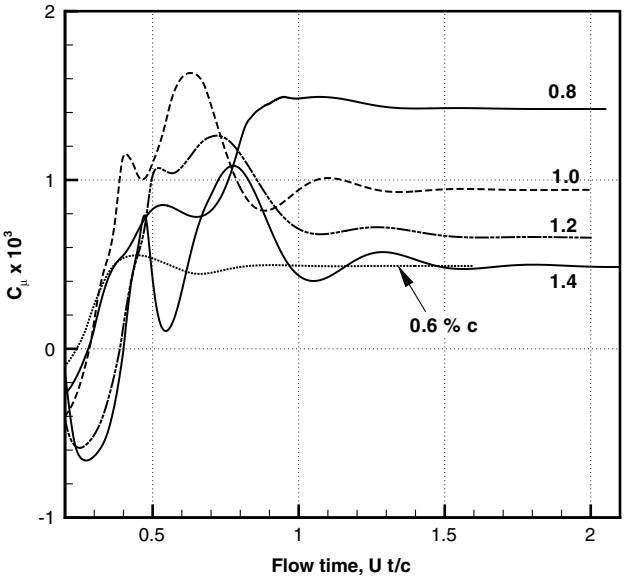

Fig. 12 Convergence history of C_μ with upper spoiler $\delta^+ = 1.4\%$ and $x_h/c = 0.70$.

The strength of the jet is relatively low and is virtually dissipated on exiting the bypass channel, due to the mixing with the incoming high-speed flow. However, the incoming external flow from the suction side does not enter the channel, but it is forced to change direction and move outward. There is an area of flow separation at the inlet of the bottom spoiler that contributes to the reduction of net throughflow in the bypass. Finally, the flow separates shortly behind the leading edge of the top spoiler.

When differential deflection is applied, the aerodynamic response changes. The convergence history for the C_μ is shown in Fig. 12. Again, the minimum flow time for a stabilized C_μ is about $Ut/c \simeq 2$, except for a case when the lower spoiler has a very small deflection. A small spoiler deflection (around 0.5% chord) causes a change in flow conditions at the inlet and a considerable reduction in net C_μ.

Figure 13a shows the velocity vectors at the exit of the channel, with the deflection of the top spoiler fixed at $\delta^+/c = 1.4\%$. The flow characteristics on this side are not affected by the differential deflection on the lower side. A separation bubble is visible on the lower side of the spoiler. This separation is due to the encounter of high-speed flow coming from the suction side of the wing. The situation is reverted at the wall, where the jet meets a low-speed boundary layer and causes separation upstream of the spoiler.

The flow pattern at the inlet is shown in Fig. 13b. There is a separation bubble across the inlet surface. This separation bubble is often present and is caused by the deflection of the spoiler; the bubble, in fact, does not appear in the solution of the plain wing section at the same operational conditions. This separation bubble must be controlled by a more accurate design if loss in bypass flow has to be avoided.

Figure 14 shows the effects of differential deflection on the aerodynamic coefficients. The case refers to variable deflection of the lower spoiler for a fixed deflection of the top spoiler, as indicated in the caption. The C_μ reaches a maximum with $\delta^-/c \simeq 1\%$, as in the previous case. The C_d increases uniformly. The spoiler deflection is a stronger parameter than a change in angle of attack, although this result is evident only within the range of angles indicated in the graphs. The C_l decreases as the lower spoiler is opened up, as a result of a disruption of the flow and the consequent aft separation. From the analysis of the pressure and viscous contribution to the drag, it was found that the pressure is by far the dominant factor.

B. Position of Hinge Points

Equation (4) indicates that the theoretical jet momentum depends on the position of the leading edge of the spoilers. Losses in the channel reduce the C_μ by a factor of 10. Therefore, if the hinge point is moved forward, the viscous losses should be reduced. To investigate how much the C_μ can be reduced, a number of calculations have been carried out with hinge points moving forward and spoilers lengths decreasing. The amount of deflection is the same as in the previous cases. The first result is shown in Fig. 15. If we compare this result with that shown in Fig. 10, we conclude that the C_μ can be increased by a factor of 2, mostly by decreased losses in the bypass channel.

The calculated force coefficients are shown in Fig. 16. In particular, Fig. 16a shows that the C_μ has a minimum at an intermediate value of the hinge point and a maximum with a forward hinge point. This result is due to decreased losses in the bypass and indicates that if a high C_μ is desired, the spoilers have to be short. Figure 16b shows the lift and drag coefficients. The glide ratio for these cases is variable between 3.5 and 4.5, and it increases as the hinge point moves aft. The overall drag decreases as the hinge point moves aft (or as the channel length increases). As far as the drag is concerned, it appears that the role of the hinge point is more dominant than the length of the bypass channel. A forward hinge causes a lower L/D. Unlike the conventional spoilers, a negative C_l can only be

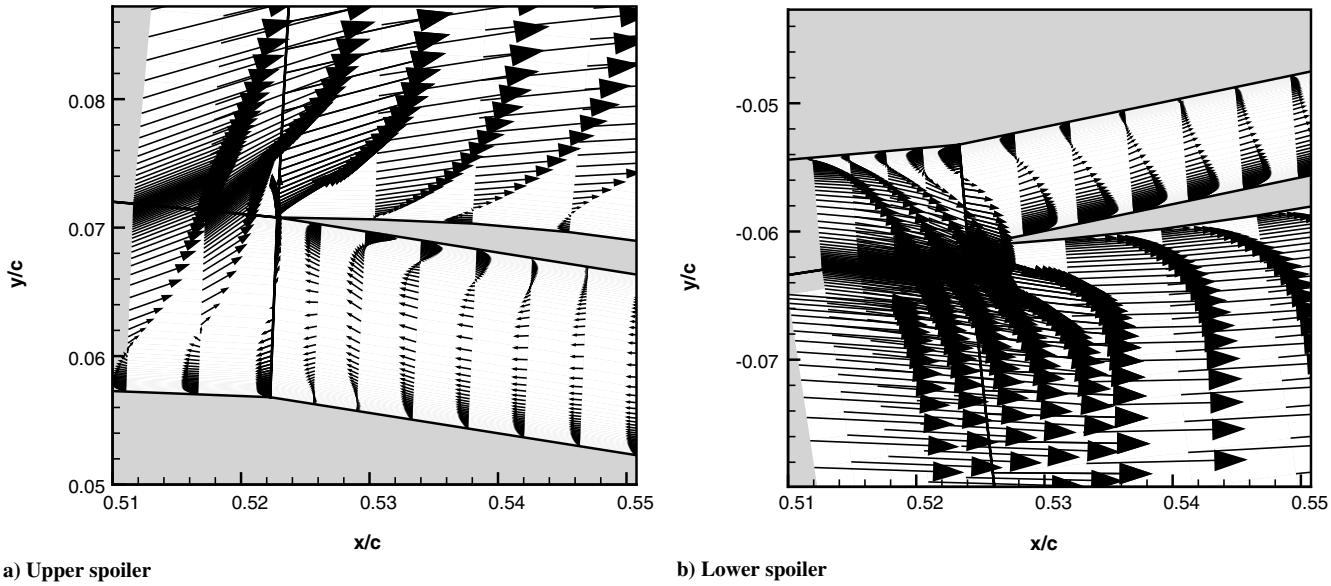

a) Upper spoiler **b) Lower spoiler**

Fig. 13 Flow characteristics at the outlet and inlet of the bypass; $\alpha = 0$ deg, $x_h/c = 0.70$, $\delta^-/c = 0.6\%$, and $\delta^+/c = 1.4\%$.

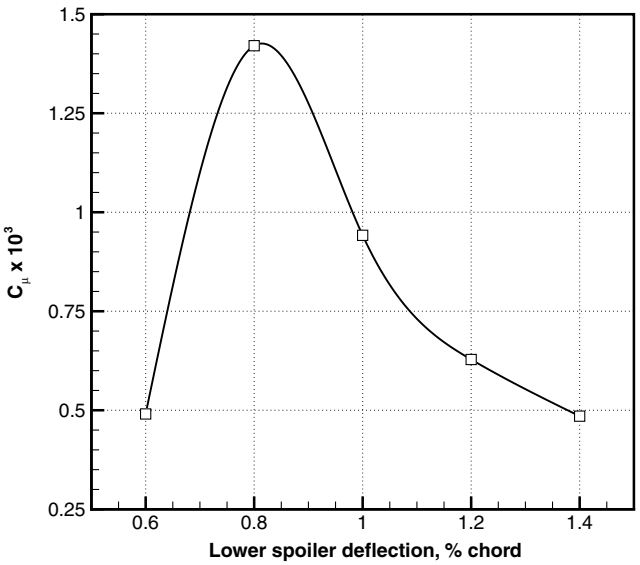

a) Jet momentum coefficient

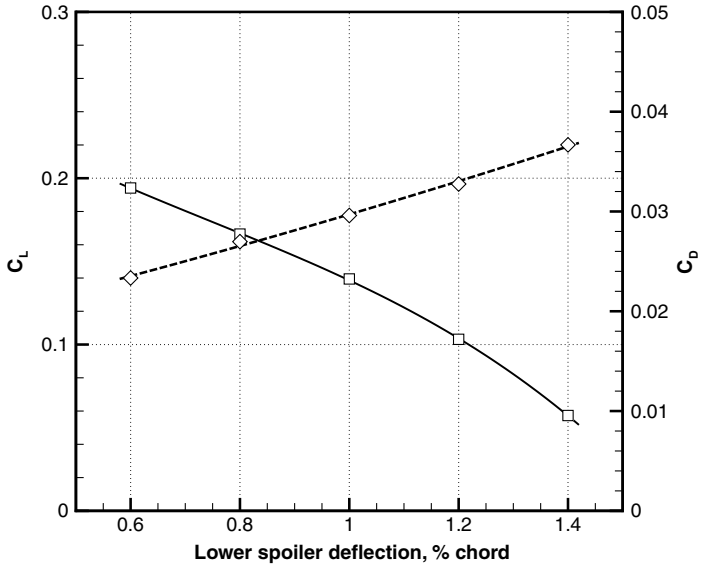

b) Aerodynamic coefficients

Fig. 14 Effects of differential spoiler deflection; upper spoiler $\delta^+ = 1.4\%$.

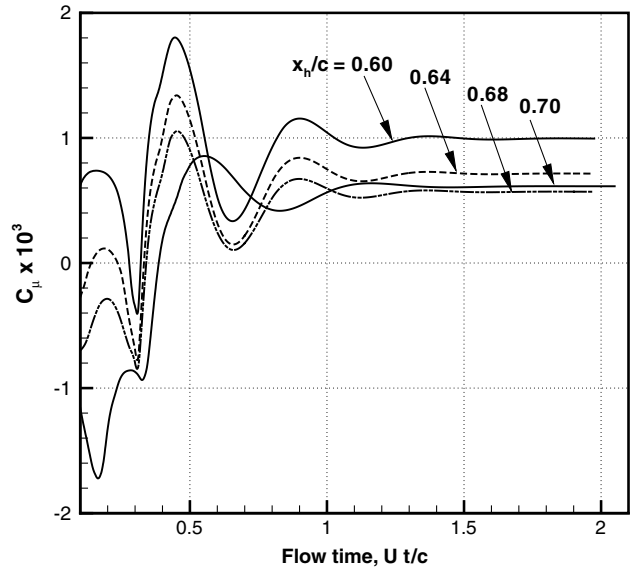

Fig. 15 C_μ history for different hinge positions; $\alpha = 0$ deg and $\delta/c = 1.2\%$.

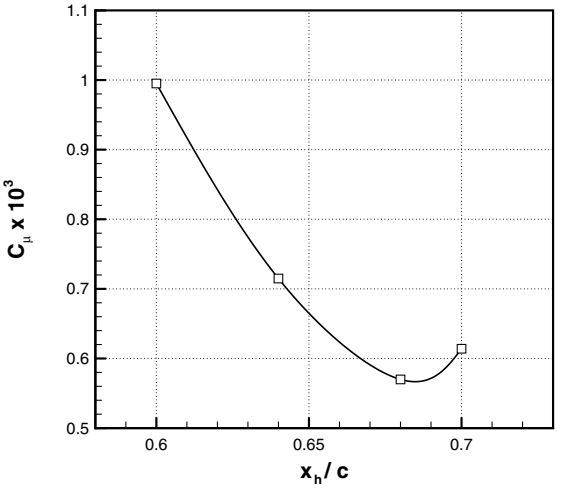

a) Jet momentum

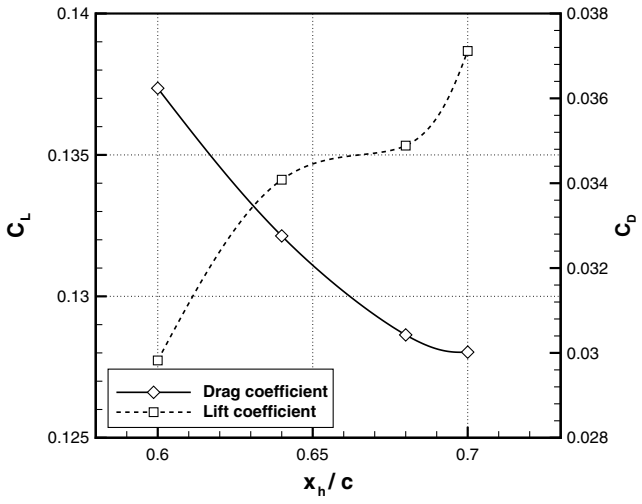

b) Lift and drag

Fig. 16 Effect of hinge point on aerodynamic coefficients.

obtained by drastically reducing the angle of attack of the wing. Alternatively, one must consider a fundamental change in the design of the spoilers, with the lower surfaces not aligned with the wing. A particular case of nonalignment is discussed in the next section.

Figure 17 shows the flow characteristics on the aft part of the wing resulting from variable position of the hinge points. The cases shown refer to the same position of the leading edge (e.g., decreasing spoiler length) and fixed deflection $\delta/c = 1.2\%$. For the shortest spoiler, there is a separation bubble S on both sides. The lower bubble virtually disappears as the hinge point moves aft, because the flow deflection decreases.

C. Slotted Bypass

The previous cases have shown the general aerodynamic performance of the spoilers for cases in which the internal surfaces are aligned with the surface of the wing. We now consider a more general case in which the deflection of the spoilers can be changed continuously. Thus, we investigated the effects of a slotted bypass for a reference configuration (fixed U-bend shape). When the spoilers are fully deflected, the internal surfaces are aligned as shown in the previous cases; otherwise, there is a backward-facing step at the inlet and a forward-facing step at the outlet. Computationally, this case is resolved by automatically adding some blocks to cover the area below the alignment point.

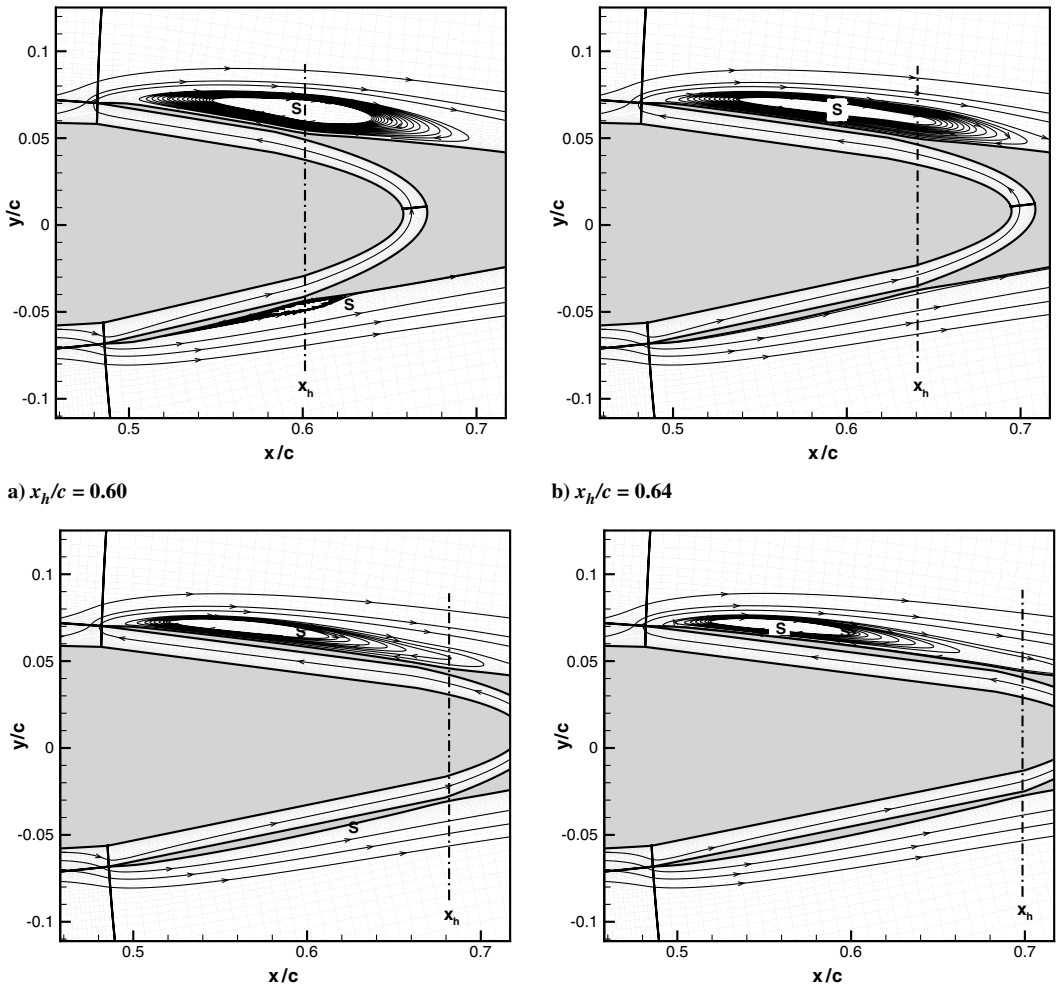

a) $x_h/c = 0.60$ **b)** $x_h/c = 0.64$

c) $x_h/c = 0.68$ **d)** $x_h/c = 0.70$

Fig. 17 Jet effects around the bypass; $\alpha = 0$ deg and $\delta/c = 1.2\%$.

This case is more challenging because it contains step changes in the cross section, which are notoriously difficult to simulate. The spoilers are allowed a maximum deflection $\delta/c = 1.2\%$, although this limit is not restrictive. The grid consisted of almost 74,000 cells, arranged in 16 blocks with $n = 68$.

Figure 18 shows a snapshot of the inlet and the outlet flow. At the inlet (Fig. 18a), there is a large separation bubble formed as a result of the backward-facing step. The separation at the outlet is more limited; the flow exits the channel with a high speed, but the jet is strongly deflected by the upstream flow. This rapid deflection is an indication of a relatively weak jet. The separation bubble downstream of the spoiler's leading edge is not affected by the new configuration.

The history of the C_μ is shown in Fig. 19 for selected cases corresponding to the same hinge position $x_h/c = 0.60$. As the deflection is increased, the net bypass mass flow increases. One case of

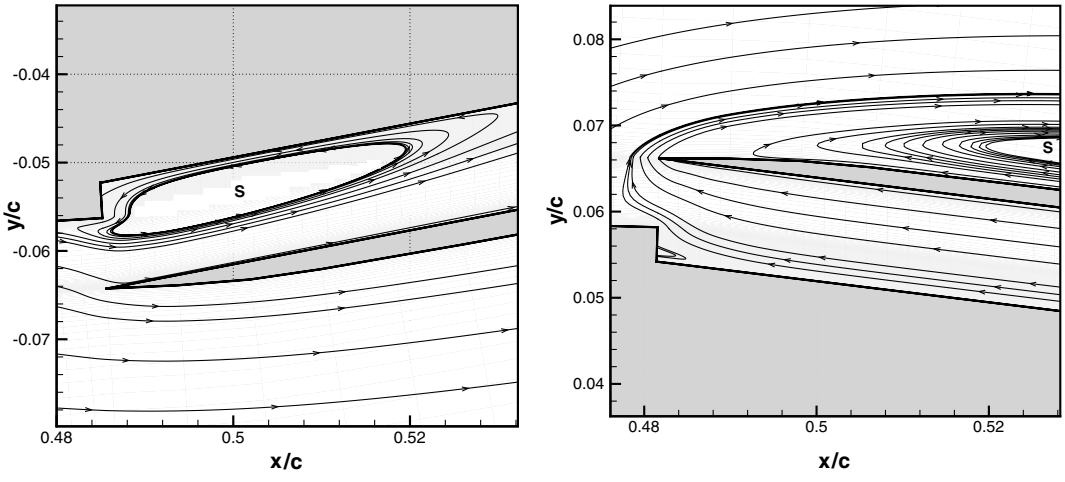

a) Lower spoiler **b) Upper spoiler**

Fig. 18 Flow characteristics at the inlet and outlet of the bypass; $\delta/c = 0.8\%$.

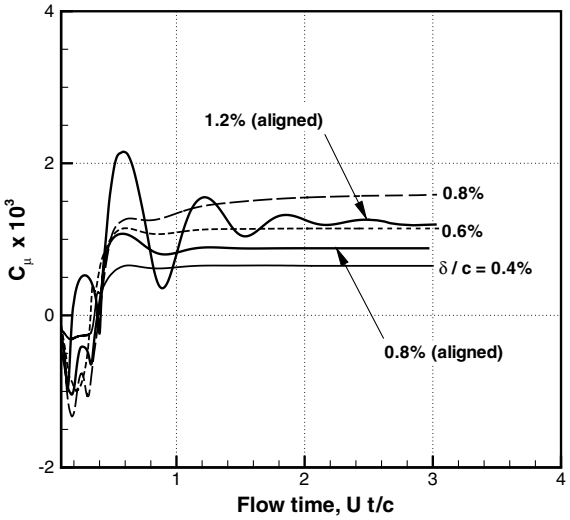

Fig. 19 Time history of C_μ with partial deflection; $x_h/c = 0.60$ and $\delta/c = 0.8\%$.

particular interest is shown in Fig. 20, which refers to a case of aligned and nonaligned internal surfaces corresponding to the same amount of deflection ($\delta/c = 0.8\%$) (also see the solid line in Fig. 19). A comparison between the respective C_μ values indicates that the slotted bypass causes a larger jet momentum. Although the exit section is the same, the slotted cavity appears to increase the net C_μ. This result is attributed to the fact that when the internal surface is not aligned, the boundary-layer effects are mitigated.

D. Role of U-Bend Shape

A portion of the viscous losses is incurred in the U-bend section of the bypass. This is not necessarily because of recirculation areas. Only small areas of backflow are present, as shown in Fig. 21 for two different geometries.

Three cases have been investigated, which are called short, medium, and long bends. These geometries were calculated by moving a control point in the Bezier spline at the center of the U-bend by $\pm 0.05c$ around a middle point. The history of the C_μ is shown in Fig. 22. The net C_μ increases as the U-bend is made shorter. In any case, only a very small flow separation is observed in the U-bend, as demonstrated by the flow analysis in Fig. 23. The external separation is unaffected by the details of the bypass. The effects on the aerodynamic coefficients are shown in Fig. 24.

E. Analysis of Control Forces

The pressure distribution across the bypass is essentially constant within the spoiler area. In any case, this pressure is considerably lower than the pressure difference inside and outside the spoilers; larger pressure gradients are found at the inlet, at the outlet, and at the U-bend. Figure 25 shows a detailed view of the external pressure distribution. The graph indicates that there is a suction peak behind both leading edges. As a result, the spoilers would tend to open up, unless they are prevented from doing so by the internal control system. In other words, once the spoilers are deflected by a small amount, they would tend to open further as a result of the aerodynamic pressures. Another factor is that the bypass flow resists the change of direction. Thus, the role of the internal control system is reverted from exerting outward pressure to exerting inward pressure.

Note that in Fig. 25 the C_p is nearly constant along the surface of the bypass. Furthermore, there is a strong pressure jump across the inlet and the outlet surfaces. The difference in pressure at the outlet (upper spoiler) is relatively large; the spoiler would tend to snap up, unless a stable control system is applied. A further analysis of the data shows that most of the hinge moment arises from the suction peak at the leading edge of the spoilers.

With reference to Fig. 26, we can safely assume that the normal pressure gradient inside the bypass $\mathrm{d}p/\mathrm{d}\eta$ is negligible ($p_1 \simeq p_2$). Hence, the pressure $\Delta p_{23}(\xi)$ acts on the lower wall of the bypass. If p_o is the pressure inside the wing (around the control system and the hinges), the total force applied to a spoiler is

$$F = \int [\Delta p_{23}(\xi) - p_o]\mathrm{d}\xi \tag{6}$$

where the integration is extended from the hinge point to the leading edge of the spoilers. The hinge moments are

$$M^+ = \int F^+ \xi \mathrm{d}\xi, \qquad M^- = \int F^- \xi \mathrm{d}\xi \tag{7}$$

The pressure p_o is unknown; therefore, it is useful to consider the hinge moment on the outer walls only, by integrating the load due to the pressure difference Δp_{23}.

Figure 27 shows the calculated hinge moments (in the absolute value) for the upper walls of the spoilers for the case discussed in Fig. 17 (effects of hinge position).

F. Comparison with Inlay Spoilers

A correlation between the new spoilers and the inlay spoilers can be done in terms of control forces required to produce specified

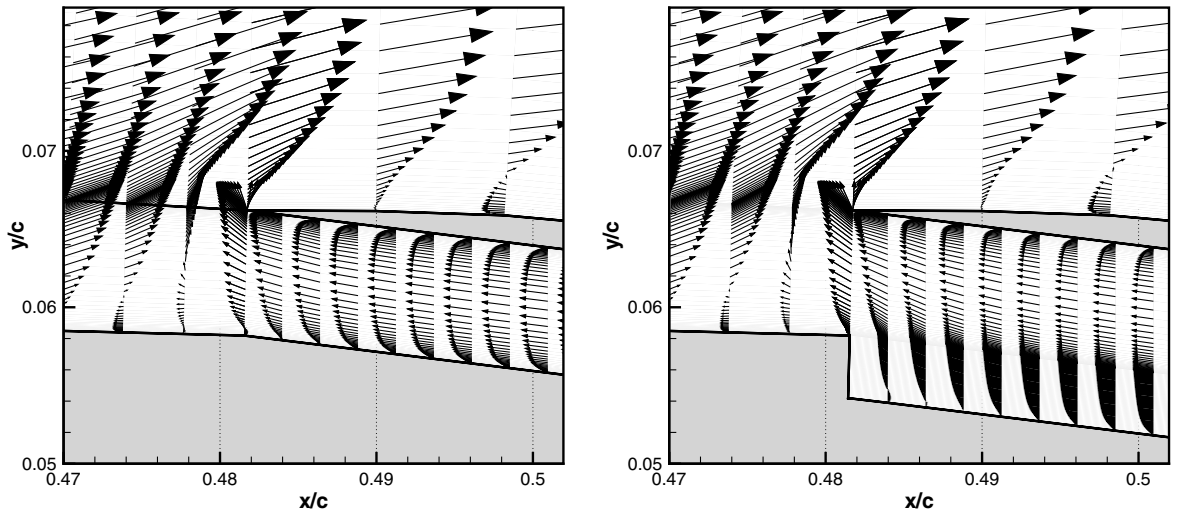

a) Simple bypass **b) Slotted bypass**

Fig. 20 Flow characteristics at the outlet of the bypass case of Fig. 19.

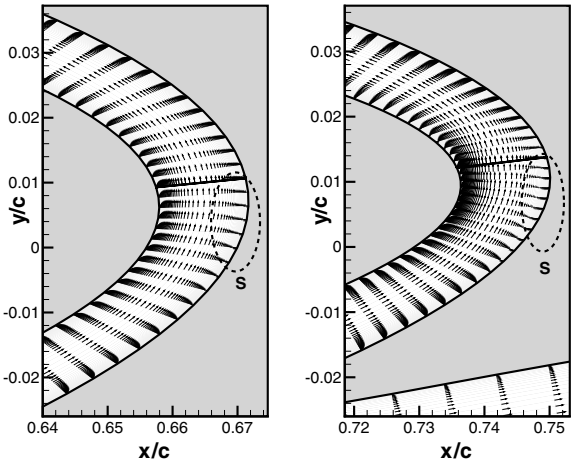

Fig. 21 Velocity vectors in the U-bend; $\alpha = 0$ deg and $\delta/c = 1.2\%$.

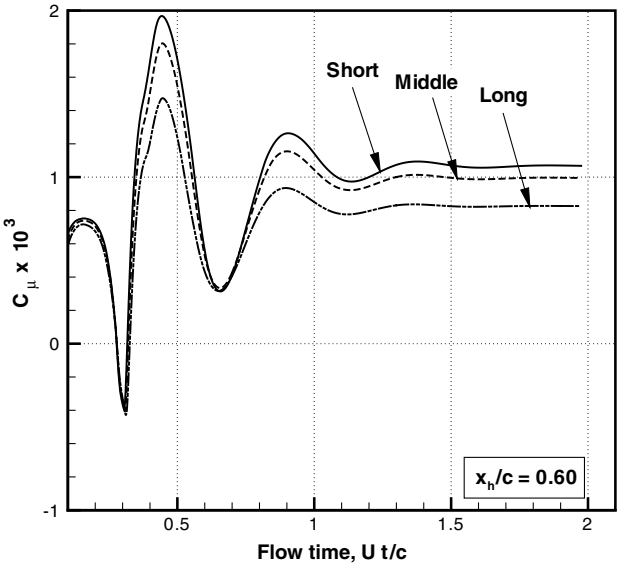

Fig. 22 Effect of U-bend shape on jet momentum coefficient.

aerodynamic coefficients. For this purpose, we need to make some assumptions on how the spoilers are operated. The model presented in this study and the conventional spoiler are fundamentally different, because the jet spoiler does not generally produce a negative lift; by contrast, an inlay spoiler, by disrupting the flow aft its panel, can create a large downforce for large panel deflections.

The distribution of base pressure behind the spoiler appears to be affected by the type of airfoil and the dimensions of the spoiler. For example, Lee and Bodapati [9] showed results in which the C_p behind the spoiler is virtually constant for a wide range of deflections; Consigny et al. [10] showed a gradual pressure recovery at the surface. The calculations shown earlier (Fig. 8) are in agreement with these findings; in particular, they indicate that the surface pressure recovers rapidly and that the base pressure remains nearly constant. However, there are rapid variations of pressure at the spoiler's leading edge, due to the unsteady-flow separation.

The first set of experimental data [9] indicate that the spoilers provide $C_d \simeq 0.2$ and $C_l \simeq -1.0$, thus $L/D \simeq -5$, with a spoiler length of about 15.5% chord and a deflection $\delta = 20$ deg. The value of the control force and the hinge moment M_h are not available. However, the moment can be inferred with some approximation from the published data. In fact, the base pressure behind the spoiler corresponding to a given deflection is given by Lee and Bodapati [9]. For a base pressure $C_{pb} \simeq -0.85$, corresponding to a deflection $\delta = 60$ deg, the difference in pressure between the two sides of the spoiler is $\Delta p = q_\infty \Delta C_p \simeq 425$ Pa. Assuming a uniform pressure loading of the spoiler, the hinge moment would be $M_h \simeq 0.88$ Nm.

The calculation of the hinge moment for the case shown in Fig. 8 with $\delta = 20$ deg leads to a $M_h \simeq 0.19$ Nm. This value is double the control moment of the lower spoiler shown in Fig. 27 ($x_h/c = 0.60$); it is also close to the control moment for the upper spoiler.

V. Spoiler Optimization

The foregoing analysis has shown that each geometrical parameter has a different effect. To optimize the device, one should agree on a suitable objective function. The functional dependence of the objective function from the configuration parameters is

$$\text{var} = f\left(\frac{x_h}{c}, \frac{\delta}{c}, \frac{l}{c}, \text{U-bend}\right) \tag{8}$$

where var is a generic variable ($C_\mu, C_d, C_m, L/D$, etc.). We consider a subspace in which the hinge points, the deflections, and the lengths are the same for the lower and upper spoilers. The U-bend geometry is limited to one parameter (a Bezier coefficient) that fully defines its shape and length. In a first-order analysis, the role of this parameter is clear: as the length increases, the C_μ decreases. Therefore, it appears useful to consider a minimal shape before the optimization process is started; this strategy should reduce the size of the search space.

There are essentially two methods for carrying out this optimization: first, by using a gradient method around a reference point;

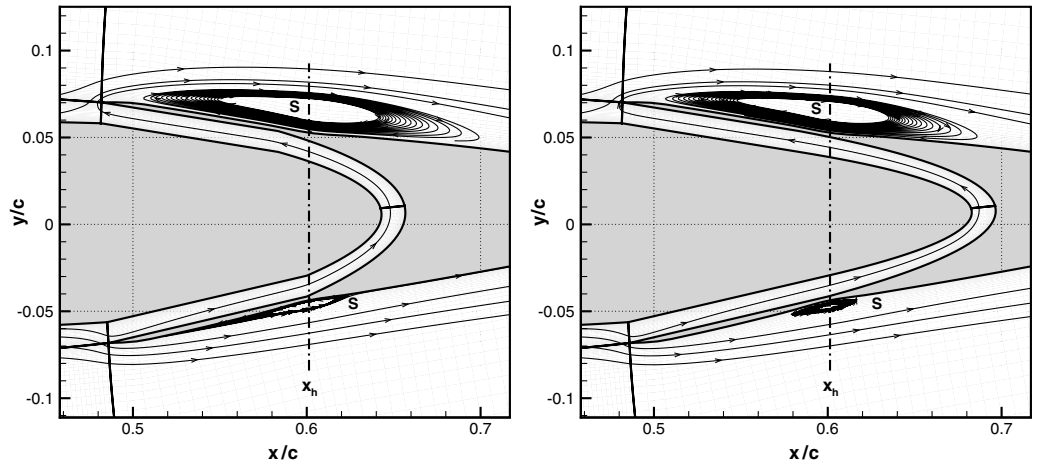

a) Short U-bend **b) Long U-bend**

Fig. 23 Effect of U-bend shape on airfoil flow; $\delta/c = 1.2\%$ and $x_h/c = 0.60$.

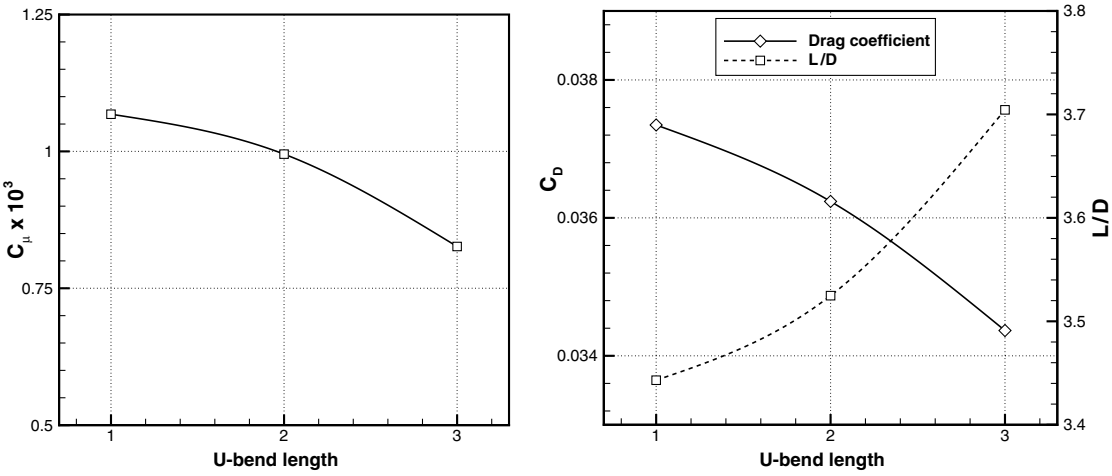

a) Jet momentum **b) Lift and drag**

Fig. 24 Effect of U-bend shape on the aerodynamic coefficient case of Fig. 23.

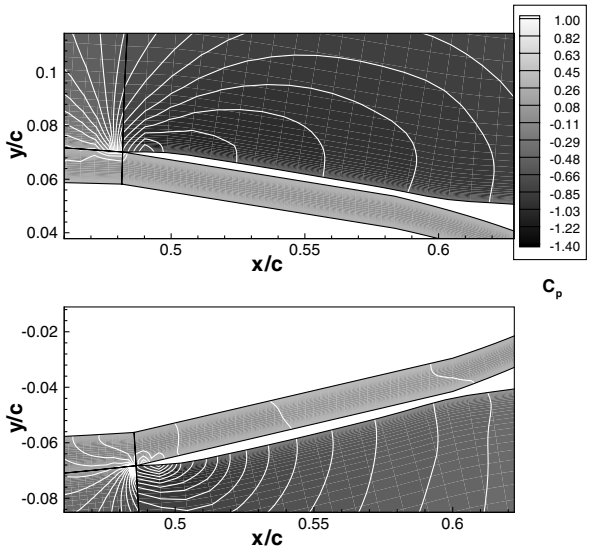

Fig. 25 External pressure distribution case of Fig. 15.

second, by calculating the spoilers within a matrix in the design space.

The gradient method must be robust enough to handle all sorts of meshes. It also requires the calculation of three sensitivities around the reference configuration to advance one step further (for example, by the steepest ascent/descent path). Convergence to an extremal point cannot be guaranteed in a specified number of steps (e.g., a fixed number of URANS computations), and occasionally the flow solver diverges. This event invalidates the process and requires a restart of the whole procedure.

By contrast, the matrix search method requires the calculation of the spoilers at selected configuration points and a higher-order interpolation within the matrix to extract limiting configurations. The method requires a relatively large number of configuration points to begin with, but to its advantage, there is the fact that minima and maxima can be analyzed for more than one parameter by using the same set of calculations; thus, it turns out to be more efficient. This approach was used in the present study. A set of 60 spoiler configurations has been defined, with configuration parameters defined by the limits

$$0.54 < x_h/c < 0.70, \qquad 0.60 < \delta/c < 1.40, \qquad 0.38 < x_{\mathrm{LE}}/c < 0.60$$

Slotted cavities, such as those discussed in Sec. IV.C, have been considered; a deflection $\delta/c = 1.40$ refers to a fully open slot with the lower lips aligned with the wing's surface. Note that these

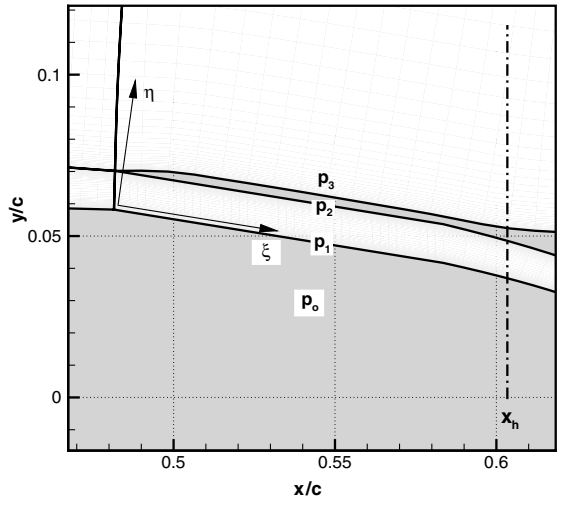

Fig. 26 Local reference system on the bypass channel.

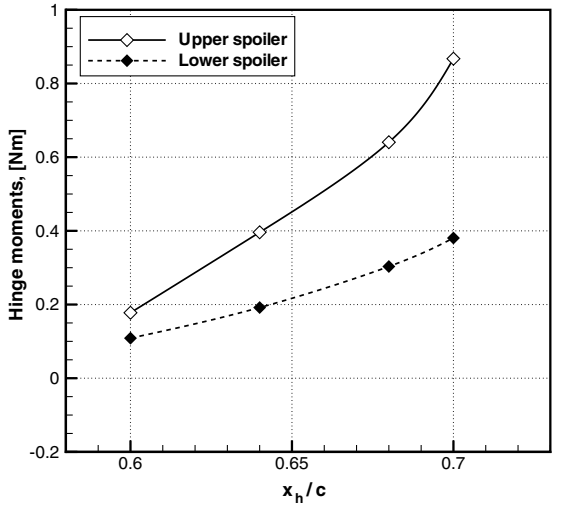

Fig. 27 Calculated hinge-moment case of Fig. 17.

Table 1 Minima and maxima resulting from the optimization matrix

Parameter	Value	x_h/c	x_{LE}/c	l/c	$\delta/c\%$
Maximum $C_\mu \times 10^3$	2.22724	0.64	0.56	0.08	1.40
Maximum C_d	0.06013	0.54	0.46	0.18	1.40
Maximum L/D	0.01109	0.54	0.46	0.18	1.40
Minimum C_m	-0.00007	0.54	0.38	0.16	1.40
Maximum C_m	0.02642	0.70	0.60	0.10	1.40

configurations cannot have the same shape as the U-bend because of the variable hinge points. All of the cases were run until the initial transient was stabilized. A few cases diverged and required a change in the underrelaxation parameters.

The optimal solutions on the raw data (e.g., the selected points in the matrix) are reported in Table 1. In all of the cases considered, the extremal values were obtained with fully open spoilers ($\delta/c=$ 1.4%). This result was attributed to the effect of the slotted cavities, which appear to produce suboptimal solutions. For example, minimum pitching moment and minimum glide ratio are both obtained with a forward hinge point and a long spoiler (forward leading edge). The configuration of maximum C_d is not the same as the configuration of maximum C_μ.

The optimization matrix was interpolated by using multidimensional cubic splines. For a given deflection, a transfinite interpolation was carried out on the search carpet x_h and x_{LE} to provide additional points on a much larger matrix. Then a bidirectional cubic spline was applied to interpolate the objective function on this carpet. Figures 28 and 29 show three-dimensional plots of the C_μ and C_d, respectively. An alternative plot would present the length of the spoiler l/c instead of the position of the spoiler's leading edge x_{LE}/c. The transformation is given by the difference $l/c = (x_h - x_{\mathrm{LE}})/c$.

Figure 28 shows levels of constant C_μ, which translate into a nonlinear relationship between the hinge point and the length of the spoiler for a fixed value of the deflection. The largest jet momentum is obtained with a configuration having an aft hinge point and short spoiler length (aft x_{LE}/c). The lowest jet momentum is obtained with the forward hinge point.

An analysis of the drag characteristics is shown in Fig. 29. Predictably, the maximum drag is obtained with a forward hinge point and a long spoiler. However, the behavior of the drag on the solution matrix is somewhat more complicated than the jet momentum. In fact, a local minimum is found at intermediate spoiler lengths *and* a forward hinge point. If the hinge is placed aft, the maximum drag is obtained with a long spoiler.

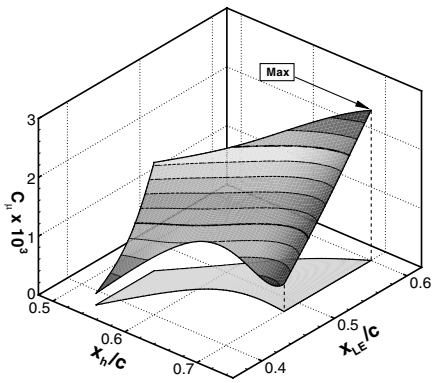

Fig. 28 Extrapolated values of C_μ on the optimization carpet.

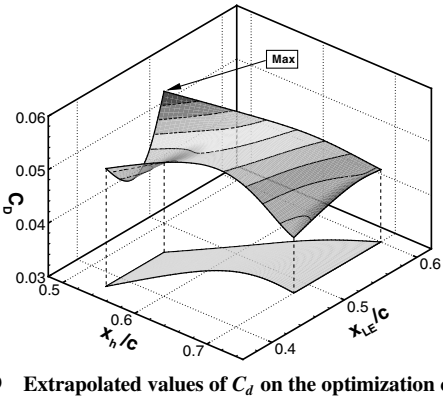

Fig. 29 Extrapolated values of C_d on the optimization carpet.

VI. Conclusions

In this paper we have proposed a new aerodynamic control device for a generic fixed-wing aircraft. The device consists of inverted upper/lower spoilers and a bypass channel. The deflection of the upper and lower spoilers is synchronized. For the configuration shown, only deflections of the order of 1% chord are possible. Thus, the device is a flow control system that requires minimum deflection of solid surfaces: an advantage that can be a requirement for certain types of aircraft. However, the system can be designed to allow a greater amount of deflection. Both lateral and longitudinal control can be achieved by appropriate deflection of right- and left-wing spoilers.

A jet flow is created by natural differences in pressure over a wide range of angles of attack. It was found that the exit jet occurs in most conditions, except at large negative angles of attack. The jet momentum coefficient is of the order of 10^{-3} or less, if the configuration is suboptimal. In any case, the jet is not clearly identified in the numerical solution, because it is relatively weak. This result is attributed to losses in the bypass channel and to the fact that the jet is powered by natural pressure differences, rather than external power. By contrast with other control techniques, the jet does not require an external power source, but at the same time, only a weak parallel jet can be produced.

The jet momentum coefficient depends on three basic parameters: the difference in pressure between lower and upper sides, the extent of the bypass channel, and the deflection. To increase the drag, it is necessary to place the hinge point in the forward position. The length of the bypass channel and the shape of the U-bend affect both the momentum coefficient and the overall drag. Properly designed, the U-bend should not give rise to significant flow separation. A comparison with inlay spoilers has been carried out. The analysis of the control moments at the hinge points demonstrated that the jet spoilers tend to open up as a result of the pressure difference between the internal and the external flow. Once deflected by a small amount, the control system has to invert the control force to maintain the deflection. The calculations indicate that the hinge moments are lower than those corresponding to a conventional inlay spoiler. However, they also change sign as the spoilers are deflected; once the spoilers are opened, for even relatively small deflections, an inward control force must be exerted. Glide ratios of the order of a few units are obtained with most deflections and configurations. Negative glide ratios cannot be achieved, unless the angle of attack is decreased by a large amount.

A final study dealt with the optimization of the jet spoilers. Starting from configurations having a slotted bypass, a full parametric study was performed. In particular, the matrix approach has allowed to carry out an analysis on multiple parameters and to refine the optima by higher-order interpolation of selected configurations.

It is emphasized that the device has been studied in static configurations (e.g., when the opening and closing of the spoilers has reached a final position). However, the transient effects could be critical and need detailed study. A further study is required to investigate the possibility of a deadband of actuation (e.g., that situation in which a very small deflection of the spoilers does not produce a sensible control force or moment). Finally, a system-engineering study is required to evaluate the application of the spoilers on an aircraft, as well as the power and actuators requirements.

References

[1] Blake, W., "Wing-Mounted Aircraft Yaw Control Device," U.S. Patent 6,491,261, issued Dec. 2002.

[2] Clark, W. D., "Aircraft with Forward Opening Inlay Spoilers for Yaw Control," U.S. Patent 6,892,982, issued May 2005.

[3] Tavella, D. A., Wood, N. J., Lee, C. S., and Roberts, L., "Two Blowing Concepts for Roll and Lateral Control of Aircraft," NASA TR CR-1804478, Oct. 1986.

[4] Tavella, D. A., Lees, C. S., Wood, N. J., and Roberts, J., "The Jet Spoiler as a Yaw Control Device," *Journal of Aircraft*, Vol. 24, No. 9, Sept. 1987, pp. 611–615.
doi:10.2514/3.45485

[5] Cyrus, J. D., Kadlec, E. G., and Klimas, P. C., "Jet Spoiler Arrangement for Wind Turbine," U.S. Patent 4,504,192, issued Mar. 1985.

[6] McClure, P. D., "Passive jet spoiler for yaw control of an aircraft," U.S. Patent 7,143,983, issued Dec. 2006, (Lockheed Martin Corp.).

[7] Costes, M., Gravelle, A., Philippe, J. J., Vogel, S., and Triebstein, H., "Investigation of Unsteady Subsonic Spoiler and Flap Aerodynamics," *Journal of Aircraft*, Vol. 24, No. 9, Sept. 1987, pp. 629–637.
doi:10.2514/3.45488

[8] Sun, X. D., Woodgate, K. G., and Allwright, J. C., "Non Linear Inverse Dynamics Control of Aircraft Using Spoilers," *Journal of Guidance, Control, and Dynamics*, Vol. 19, No. 2, Mar. 1996, pp. 475–482.
doi:10.2514/3.21642

[9] Lee, C. S., and Bodapati, S., "Experimental Investigations of the Flowfield of an Airfoil with Spoiler," *AIAA Journal*, Vol. 25, No. 11, May 1987, pp. 1411–1416.
doi:10.2514/3.9797

[10] Consigny, H., Gravelle, A., and Molinaro, R., "Aerodynamic Characteristic of a Two-Dimensional Moving Spoiler in Subsonic and Transonic Flow," *Journal of Aircraft*, Vol. 21, No. 9, Sept. 1984, pp. 687–694.
doi:10.2514/3.45015

[11] Filippone, A., "Steep-Descent Maneuver of Transport Aircraft," *Journal of Aircraft*, Vol. 44, No. 5, Sept. 2007, pp. 1727–1739.
doi:10.2514/1.28980

[12] Michelsen, J. A., "Block Structured Multigrid Solution of 2D and 3D Elliptic PDE's," Technical Univ. of Denmark, Dept. of Mechanical Engineering, AFM TR 94-06, Lyngby, Denmark, 1994.

[13] Scrensen, N. N., "General Purpose Flow Solver Applied over Hills," Risø National Lab. TR RISØ-R-827-(EN), Roskilde, Denmark, 1995.

[14] Sørensen, N. N., Michelsen, J. A., and Schreck, S., "Navier–Stokes Prediction of the NREL Phase VI Rotor in the NASA Ames 80 ft × 120 ft Wind Tunnel," *Wind Energy Technology*, Vol. 5, Nos. 2–3, Apr.–Sept. 2002, pp. 151–169.

[15] Filippone, A., and Michelsen, J. A., "Aerodynamic Drag Prediction on Helicopter Fuselage," *Journal of Aircraft*, Vol. 38, No. 2, Mar. 2001, pp. 326–333.
doi:10.2514/2.2765

[16] Filippone, A., "Prediction of Aerodynamic Forces on a Helicopter Fuselage," *The Aeronautical Journal*, Vol. 111, No. 1117, Oct. 2006, pp. 175–184.

[17] Choi, S. W., Chang, K. S., and Ok, H., "Parametric Study of Transient Spoiler Aerodynamics with Two-Equation Turbulence Models," *Journal of Aircraft*, Vol. 38, No. 5, Sept. 2001, pp. 888–894.
doi:10.2514/2.2848